In the 3rd International Workshop, EMMCVPR, Sep. 2001, France, pp. 544-559

A Continuous Shape Descriptor by Orientation Diffusion *

Hsing-Kuo Pao Davi Geiger

Courant Institute, New York University, New York, NY 10012, USA,
212-9983485 212-9983235
hsingkuo@cs.nyu.edu geiger@cs.nyu.edu

Abstract. We propose a continuous description for 2-D shapes that calculates convexity, symmetry and is able to account for size. Convexity and size are known to be critical in deciding figure/ground (F/G) separation, with the study initiated by the Gestalt school [9] [11]. However, few quantitative discussions were made before. Thus, we emphasize the convexity/size measurement for the purpose of F/G prediction. A Kullback-Leibler measure is introduced. In addition, the symmetry information is studied through the same platform. All these shape properties are collected for shape representations. Overall, our representations are given in a continuous manner. For convexity measurement, unlike the $1/0$ mathematical definition where shapes are categorized as convex or concave, we give a measure describing shapes as "more" or "less" convex than others. In symmetry information (skeleton) retrieval, a 2-D intensity map is provided with the intensity value specifying "strength" of the skeleton. The proposed representations are robust in the sense that small fine-scale perturbations on shape boundaries will cause minor effects on the final representations. All these shape properties are integrated into one description. To apply to the F/G separation, the shape measure can be flexibly chosen between a size-invariant convexity measure or a convexity measure with the small size preference. The model is established on an orientation diffusion framework, where the local features, served as inputs, are intensity edge locations and their orientations . The approach is a variational one, rooted in a Markov random field (MRF) formulation. A quadratic form is used to assure simplicity and the existence of solution.

1 Introduction

The convexity criteria has been argued to be important in F/G separation (Kanizsa [9] or Fig. 1), where a 2-D region can be recognized as figure due to the convexity property of its borders. However, the measurement for convexity was left as intuitive and no formalism was then offered. The mathematical definition of convexity** only allows for two class of shapes: convex or concave ones (not convex). There is an intuition that some shapes are "more convex" than others (Fig. 1 (a1) (a2), Fig. 6 (a1)-(a3)). To capture this intuition, we study a continuous measure of convexity.

* Key Words: Early Vision, Shape Analysis, Convexity, Symmetry, Orientation Diffusion.

** A shape is convex if given any pair of interior points, the segment connecting these points is completely inside the shape

(a1) (a2) (b1) (b2)

Fig. 1. The preference of convexity and size. In (a1)/(a2), white/black regions are reported as figures respectively which argues convexity playing an important role in such a decision. In (b1), white strips are likely to be perceived in front of black background which gives an example of (small) size preference.

First, the human visual system tends to ignore minor perturbation (protrusion) of shapes. Such robustness is therefore a desired feature for a model measuring convexity. By a measure with this consideration, figural regions can be selected. We will argue that this F/G selection can not be provided by a well-known continuous criteria, called *shape compactness*, defined by the ratio of the square of perimeter to the shape area [1]. A related topic is to study a size-invariant measure. Under this measure, shapes can be compared to each other, for shapes with or without similar size. However, because the human visual system prefers small size objects to be perceived as figures (Koffka [11], Fig. 1(b1) (b2)), our complete model of shapes should also be able to measure convexity integrated with a preference of small size shapes. Our model will provide a parameter that can be tuned to a size-invariant convexity measure or one that biases towards small size shapes.

We propose an orientation diffusion process defined in the space $\mathbf{R}^2 \times \mathbf{S}^1$. In our view, the elements/features detected at images at the first stage are intensity edge locations and their orientations. It is known that human visual perception is based on orientation filters (found in area V1 and V2 of the brain), providing the orientation of the edges detected. Afterwards, a scheme is designed by a computation of propagating the oriented boundary information through *local interactions*. The problem of propagation is formulated as a Markov random field. By our model, the problem of F/G can be studied in a wide range of imagery.

Besides the convexity measurement, the symmetry information (skeleton) can be derived through the computation of divergence of a vector field which is generated from the result of orientation diffusion. Overall, our model is able to (i) deliver simultaneously a convexity measure and symmetry information of shapes; (ii) adjust (via one parameter) the balance between convexity and size, i.e., it is able to bias to a size invariant model or to include size in its measure.

1.1 Previous Work

Mumford [13] used *Elastica* in the smooth curve finding. The line propagation was done via a diffusion process in orientation and a translation in the $(\cos\theta\frac{\partial}{\partial x} + \sin\theta\frac{\partial}{\partial y})$-direction (with an exponential decay). Therefore, our model is similar to his. The most important difference is that our consideration is made in $\mathbf{R}^2 \times \mathbf{S}^1$ rather than in $\mathbf{R}^2$, causing all orientations to be considered simultaneously in a minimization formulation. Also, we are proposing various shape measures, a topic beyond his work.

Another interesting technical work was given by Tang et al. [20]. They were only concerned with smoothing dense vector field. A technical difference is that their work was done in the space of maps with a unit vector for each 2-D point, while we work on the space of $\mathbf{R}^2 \times \mathbf{S}^1$. Their *direction diffusion* was used for image processing and noise removal. We use a different diffusion process to generate a field based on a local sparse input. Also, we are interested in obtaining various measures to describe 2-D shapes, by investigating this field.

Pao et al. [16] have proposed a continuous measure of convexity (let us call it the PGR model). However, various problems exist with their model, perhaps the most serious one is that the size of shapes dominates the convexity measure and so small concave shapes could be preferred over larger circles. Thus, not only the model did not separate convexity from size, but also the dominance of size might not be desired.

The work on diffusion and shapes by Kimia, Tannenbaum & Zucker [10] and Siddiqi & Kimia [19] are sources of inspiration. The main difference here is that we are examining a linear diffusion equation on a more complex space of positions and orientations. For searching the skeleton of a shape, we compute the “sinkage” of energy in the shape. It is similar to Dimitrov et al. [4], with the computation of divergence of a vector field. Although, our vector field is generated by a different method.

2 Orientation Diffusion

Given a 2-D region/shape Ω (boundary and its inside), or its boundary $\partial\Omega$, we discuss its convexity and other shape properties. The region/shape or its boundary can be complete, or partial where only part of it is visible through the image frame. We use Γ instead for the boundary when the shape/boundary is partially visible. On the boundary, the orientation information can be locally represented by unit normal vectors in the inward directions (Fig. 2(b1)). Given a set of detectors of the boundary and their orientations, we want to derive a field inside the boundary to describe various shape properties.

We adopt an *orientation diffusion* / *random walk* process to solve this problem. The approach is in part inspired by Kumaran et al. [12], Pao et al. [16] (PGR model or decay diffusion [15]) where their diffusion process was worked on the image space $\mathbf{I}$, and also inspired by Mumford [13], Tang [20] where they included the orientation space. We extend the PGR model to augment the space to $\mathbf{I} \times \Theta$ by adding an orientation dimension $\Theta \equiv \{\theta \cdot 2\pi/T : \theta = 0, 1, \ldots, T-1\}$.

We will show that our model can provide a more appropriate measure for convexity than previous works. Moreover, other properties of shapes such as their skeleton information will also be obtained.

2.1 Notations

For a given region Ω (represented by Γ) in an input image *** $\mathbf{I} \equiv \{\mathbf{x} = (x, y) \in \{0, \ldots, L_1 - 1\} \times \{0, \ldots, L_2 - 1\}$, a set of useful information is collected. For an in-

*** We will use **bold** face, lower-case letters to denote vectors.

tensity function $I(\mathbf{x})$, the edge function

$$e(\mathbf{x};\theta) = \frac{1}{M_e}\left|\frac{\partial I(\mathbf{x})}{\partial \mathbf{u}_\theta}\right| \in [0,1], \quad \mathbf{x} \in \Gamma$$

records the normalized magnitude of the intensity change at pixel $\mathbf{x}$ in the direction of $\mathbf{u}_\theta = (\cos\theta, \sin\theta)$; namely, the (unsigned) directional derivative in $\mathbf{u}_\theta$, normalized by $M_e = \max\{|\frac{\partial I(\mathbf{x})}{\partial \mathbf{u}_\theta}| : \mathbf{x} \in \mathbf{I}, \theta \in \Theta\}$, the largest orientational intensity edge in the image $\mathbf{I}$. Also, on Γ, a hypothesis set (or inducers) is defined by

$$\sigma_0(\mathbf{x};\theta) = \begin{cases} e(\mathbf{x};\theta) & \text{if } \mathbf{u}_\theta \cdot \mathbf{n}(\mathbf{x}) \geq 0 \ \wedge \ \mathbf{x} \in \Gamma \\ 0 & \text{if } \mathbf{u}_\theta \cdot \mathbf{n}(\mathbf{x}) < 0 \ \wedge \ \mathbf{x} \in \Gamma. \end{cases} \tag{1}$$

On the boundary, the vector $\mathbf{n}(\mathbf{x})$ is the unit normal vector chosen the inward direction. We say that the directions closer to the inward side are in the source mode and the directions closer to the outward side are in the sink mode. Finally, a field

$$\sigma(\mathbf{x};\theta) : \Omega \times \Theta \to \mathbf{R}$$

will be evaluated by our orientation diffusion process.

2.2 Variational Model

We will create an orientation diffusion process worked in the field $\{\sigma(\mathbf{x};\theta) : \mathbf{x} \in \Omega,\ \theta \in \Theta\}$ by formulating it as a variational problem.

Local Hypotheses and Data Fitting The field $\sigma(\mathbf{x};\theta)$ should take the local hypothesis values $\sigma_0(\mathbf{x};\theta)$, where they are available. In our model they are available at all intensity edge pixels (pixels on Γ) according to their strength $e(\mathbf{x};\theta)$. I.e., we seek the $\sigma(\mathbf{x};\theta)$ which minimizes

$$E_{\text{data}}(\sigma|\sigma_0) = \sum_{(\mathbf{x};\theta)\in\Gamma\times\Theta} e(\mathbf{x};\theta)\,(\sigma(\mathbf{x};\theta) - \sigma_0(\mathbf{x};\theta))^2\,. \tag{2}$$

In most cases, the gradient direction is the one with the maximum value of $e(\mathbf{x};\theta)$, associated with either an inward ($\sigma_0 \geq 0$) or outward hypothesis ($\sigma_0 = 0$).

For the homogeneous regions (where no intensity edge is present), we extend the definition of the functions σ_0 and e by respectively assigning a local hypothesis of value 0 and a small constant strength,

$$\sigma_0(\mathbf{x};\theta) = 0 \quad \text{if } \mathbf{x} \in \Omega \ \wedge \ \mathbf{x} \notin \Gamma \tag{3}$$

$$e(\mathbf{x};\theta) = \lambda \quad \text{if } \mathbf{x} \in \Omega \ \wedge \ \mathbf{x} \notin \Gamma\,. \tag{4}$$

The index of the summation in Eq. 2 becomes $(\mathbf{x};\theta) \in \Omega \times \Theta$ now, taking the whole region. The small constant parameter $0 < \lambda \ll 1$, known as the decay coefficient †, controlling the decay effect of the energy when σ is away from the inducers (hypothesis set). A larger λ has stronger effect to bring pixels away from the intensity edges to take the value 0 (See Fig. 3(d) & (e)).

† When this functional is analyzed as a Markov chain, the parameter λ plays the role of decay parameter, or the probability of "vanishing", of the random walk associated to this functional.

Smoothness Propagation of the local hypothesis is done by adding a smoothness term that prefers neighboring pixels with similar orientations sharing the similar values. For instance, in Fig. 2(a), the vector in position P_0 with the orientation θ and its neighbor P_1 with the orientation $\theta+\psi$ are encouraged to share similar value of σ. A simple quadratic form is applied here by minimizing

$$\frac{1}{\kappa}\sum_{\psi=-\kappa}^{\kappa} M(\mathbf{x};\theta,\psi)(\sigma(x+\cos\theta, y+\sin\theta, \theta+\psi)-\sigma(\mathbf{x},\theta))^2, \tag{5}$$

for each $\mathbf{x}$ and θ. The function $M(\mathbf{x};\theta,\psi)$ is simply provided by $\cos(\psi\frac{\pi}{2k})$, giving the cosine weighting for the smoothness that concentrates particularly on small deviations. A more complicated version of the function M may also depend on $\mathbf{x}$ (non-homogeneous) or θ (anisotropic). The parameter[‡] $\kappa\in(0,\pi)$, called the <u>deviation factor</u> controlling the deviation of orientations for the moving particles. A continuous version of Eq. 5 is used here for computational purposes.

$$E_{\text{smooth}}(\sigma)=\int_{\Omega\times\Theta}\left[\frac{1}{\kappa}\int_{-\kappa}^{\kappa} M(\mathbf{x};\theta,\psi)(\cos\theta\,\sigma_x+\sin\theta\,\sigma_y+\psi\sigma_\theta)^2 d\psi\right] d\mathbf{x}d\theta. \tag{6}$$

Energy Functional The total energy functional is the summation of the data fitting term (a continuous form is applied by substituting a 2-D Dirac-delta function in Eq. 2 [15]) and the smoothness term

$$E(\sigma|\sigma_0)=E_{\text{data}}(\sigma|\sigma_0)+E_{\text{smooth}}(\sigma), \tag{7}$$

where the functional $\mathcal{H}(\sigma|\mathbf{x};\theta)$ within the bracket in Eq. 6 can be abbreviated as

$$\begin{aligned}
&\mathcal{H}(\sigma|\mathbf{x};\theta)\\
&=(\cos\theta\sigma_x+\sin\theta\sigma_y)^2\cdot\frac{1}{\kappa}\int_{-\kappa}^{\kappa} M(\mathbf{x};\theta,\psi)\,d\psi\\
&\quad+2\sigma_\theta(\cos\theta\,\sigma_x+\sin\theta\,\sigma_y)\cdot\frac{1}{\kappa}\int_{-\kappa}^{\kappa}\psi M(\mathbf{x};\theta,\psi)\,d\psi+{\sigma_\theta}^2\cdot\frac{1}{\kappa}\int_{-\kappa}^{\kappa}\psi^2 M(\mathbf{x};\theta,\psi)\,d\psi\\
&=A\,(\cos\theta\,\sigma_x+\sin\theta\,\sigma_y)^2+2B\,\sigma_\theta(\cos\theta\,\sigma_x+\sin\theta\,\sigma_y)+C{\sigma_\theta}^2\,.
\end{aligned} \tag{8}$$

where $A=4/\pi$, $B=0$ and $C=4\kappa^2/\pi$. Its Euler-Lagrange equation can be given by

$$\cos^2\theta\,\sigma_{xx}+2\sin\theta\cos\theta\,\sigma_{xy}+\sin^2\theta\,\sigma_{yy}+\kappa^2(1-\frac{8}{\pi^2})\,\sigma_{\theta\theta}=\frac{\lambda\pi}{4}\sigma, \tag{9}$$

with the boundary condition $\sigma(\mathbf{x};\theta)=\sigma_0(\mathbf{x};\theta)$, if $(\mathbf{x},\theta)\in\Gamma\times\Theta$.

Numerically, the energy function is quadratic and the minimizer is straightforwardly obtained by rewriting Eq. 7 as a matrix form by the finite difference method, and solving it by a gradient-descent method. We call this minimizer $\sigma^*(\mathbf{x};\theta)$. Some examples of $\sigma^*(\mathbf{x};\theta)$ are shown in Fig. 3(a) & (b).

‡ We avoid the degenerate case, $\kappa=0$, when the smoothness functional becomes $\sum_{\mathbf{x},\theta} M(\mathbf{x},\theta,0)(\sigma(\mathbf{x},\theta)-\sigma(x+\cos\theta,y+\sin\theta,\theta))^2$, no longer depending on ψ, and the minimization process can be worked separately through different θ's.

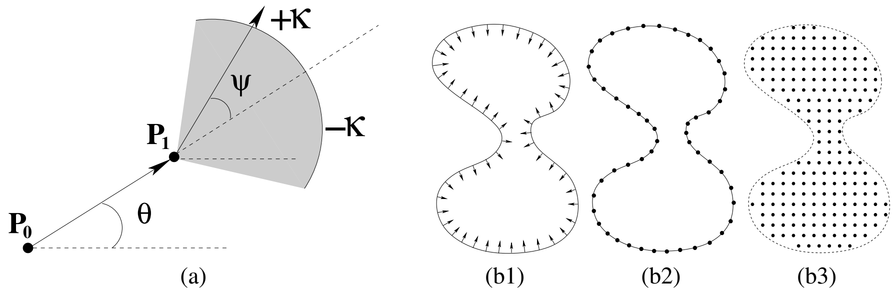

Fig. 2. (a) a particle moves from P_0 to P_1 with slightly changed in orientation. We say that the particle has the configuration changed from $(\mathbf{x};\theta)$ to $(x+\cos\theta, y+\sin\theta;\theta+\psi)$ as it goes from the point P_0 to P_1 (assume $|P_0-P_1|=1$). The shadow area indicates the possible trails that the particle may choose, with different weighting according to the deviation angle ψ. (b1) one part of the hypothesis set σ_0 (Eq. 1: part 1) with inward vectors of length $e(\mathbf{x};\theta)$ represented by vector notations. Only the normal directions are shown. Other parts includes (b2) set of vectors of length 0 with outward direction (Eq. 1: part 2) and (b3) decay vectors generally put all over the space $(\mathbf{I}-\Gamma)\times\Theta$ (Eq. 3).

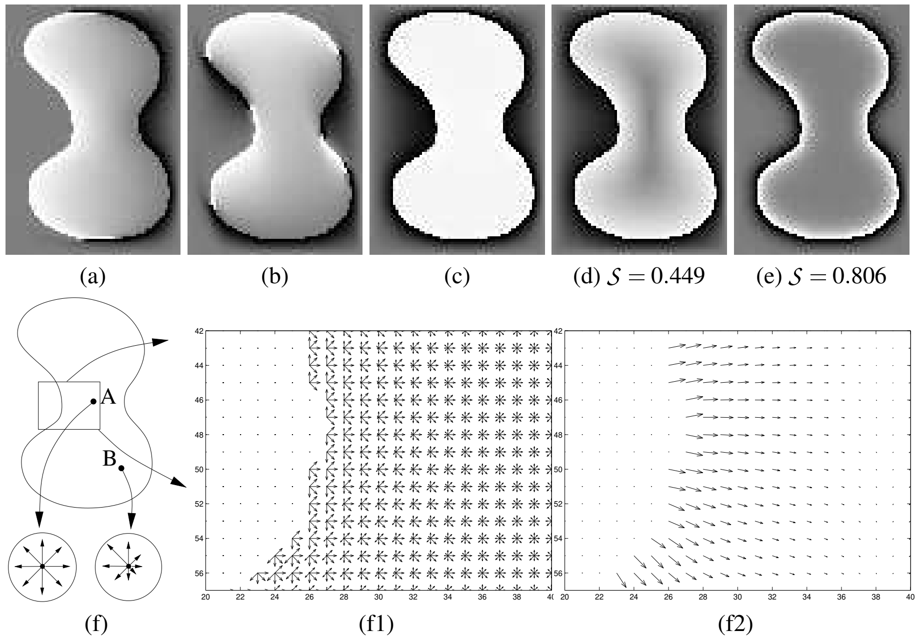

Fig. 3. Results of orientation diffusion process by two presentations. (a) $\sigma(x,y;0)$, (b) $\sigma(x,y;\frac{27}{16}\pi)$, (c) maximum magnitude among all orientations, and (d) (e) relative entropy $D(P_{\mathbf{x}}\|Q)$ (Eq. 12) with $\lambda = 0.1/|\Omega| = 2.876\times10^{-5}$, $500/|\Omega| = 0.144$ respectively. The difference shows effect of the energy decay. Larger λ gives stronger decay, less diffusion and larger convexity measure (Eq. 13). (f1) (f2) Vector presentations for part of the bell shape figure in (f). (f1) the vector bundles with choice of 8 orientations. We say that the point A has a more balanced (symmetry) result along different orientations than the bundle in B. (f2) the convexity vector $\hat{\sigma}^*$ (Eq. 10).

2.3 Kullback-Leibler Measure

Once the field $\sigma^*(\mathbf{x};\theta)$ is obtained, we can evaluate those shape properties, such as convexity or symmetry. First of all, from the solution space $\Omega \times \Theta$ to the image space Ω, we perform a vector summation considering $\sigma^*(\mathbf{x};\theta)$ as a vector in the direction of $\mathbf{u}_\theta = (\cos\theta, \sin\theta)$ with length $\sigma^*(\mathbf{x};\theta)$ (always non-negative),

$$\hat{\sigma}^*(\mathbf{x}) = \hat{\sigma}^*_{\mathrm{cv}}(\mathbf{x}) = \int_0^{2\pi} \sigma^*(\mathbf{x};\theta)\, \mathbf{u}_\theta \, d\theta\,, \tag{10}$$

where direction of the resultant vector $\hat{\sigma}^*_{\mathrm{cv}}$ will be recorded by θ^*, if it has non-zero length. We shall use $\hat{\sigma}^*$ to denote the resultant vectors if no confusion can be made. One example of the vector field $\hat{\sigma}^*(\mathbf{x})$ is in Fig. 3(f2). The idea is that this vector summation will remove the symmetry information of the solution field, and thus what is left is "convexity". For example, the center of a circle is perfectly symmetric and will result in $\hat{\sigma}^* = \mathbf{0}$ while other internal points will have the symmetry removed and still produce evidence of convexity. In our approach, convexity works on the complementary information as symmetry does. Detecting symmetry will be done by investigating which coordinates have a vector summation yield zero value (cancellations), while convexity examines the non-zero valued information of the vector summation. Indeed, the convexity measure we propose measures how well the "vector bundle" is accumulated around this summation vector. Let us be more precise.

At a fixed location $\mathbf{x}$, for each pair of opposite orientations θ and $\theta + \pi$, we compute the net effect, called the map $\tau^*(\mathbf{x};\theta)$ by

$$\begin{aligned}
\tau^*(\mathbf{x};\theta) &= \frac{1}{2}\{\sigma^*(\mathbf{x},\theta) - \sigma^*(\mathbf{x},\theta+\pi) + |\sigma^*(\mathbf{x},\theta) - \sigma^*(\mathbf{x},\theta+\pi)|\} \\
\tau^*(\mathbf{x};\theta+\pi) &= \frac{1}{2}\{\sigma^*(\mathbf{x},\theta+\pi) - \sigma^*(\mathbf{x},\theta) + |\sigma^*(\mathbf{x},\theta+\pi) - \sigma^*(\mathbf{x},\theta)|\} \\
&= \tau^*(\mathbf{x};\theta) - \sigma(\mathbf{x};\theta) + \sigma(\mathbf{x};\theta+\pi)\,,
\end{aligned} \tag{11}$$

where a cyclic boundary condition $\theta = \theta + 2\pi$ is used. Note that Eq. 10 can be rewritten as $\hat{\sigma}^*(\mathbf{x}) = \int_0^{2\pi} \tau^*(\mathbf{x};\theta)\, \mathbf{u}_\theta \, d\theta$. The second step is to transform $\tau(\mathbf{x};\theta)$ to $P^*(\mathbf{x};\theta)$ or simply $P_{\mathbf{x}}(\theta)$, by a linear transformation. It is

$$P^*(\mathbf{x};\theta) = \frac{1}{2}(1 + \tau^*(\mathbf{x};\theta))\,.$$

Unlike any previous work, we propose a Kullback-Leibler distance (or relative entropy) to measure convexity. The map $P_{\mathbf{x}}(\theta)$ is compared to a Gaussian map in $\mathbf{S}^1$ (not normalized)

$$Q(\theta) = \frac{1}{1+\varepsilon_N} \exp\left(-\frac{(\theta - \theta^*)^2}{2 \cdot (2.0)^2}\right), \qquad -\pi \le \theta \le \pi$$

where the center of Q is located in the direction θ^*, the direction of vector $\hat{\sigma}^*$. A small positive constant ε_N is added to avoid the case of $Q(\theta) = 1$. The Kullback-Leibler distance, computed at every point $\mathbf{x}$, between $Q(\theta)$ and $P_{\mathbf{x}}(\theta)$ is given by

$$D(P_{\mathbf{x}} \| Q) = \int_0^{2\pi} P_{\mathbf{x}}(\theta) \log \frac{P_{\mathbf{x}}(\theta)}{Q(\theta)} + (1 - P_{\mathbf{x}}(\theta)) \log \frac{1 - P_{\mathbf{x}}(\theta)}{1 - Q(\theta)}\, d\theta\,. \tag{12}$$

Intuitively, it measures the inefficiency of assuming that the distribution is $Q(\theta)$ when the real distribution is $P_{\mathbf{x}}(\theta)$. That is, we assume the map in $\mathbf{S}^1$ has a sharp peak at θ^*. $D(P_{\mathbf{x}}\|Q)$ is always equal to or greater than 0, and it can be greater than 1. A smaller measure means a better fit.

This measure is given for each point $\mathbf{x}$. To obtain a global measure of a shape, we simply average this measure over the points on the figure. I.e., the final measure of a shape Ω is

$$\mathcal{S}(P_{\mathbf{x}}) = \frac{1}{|\Omega|}\int_{\Omega} D(P_{\mathbf{x}}\|Q)\,d\mathbf{x}\,, \tag{13}$$

A shape with a smaller measure is considered more convex than others. A simple example can be seen in Fig. 4 as a F/G experiment. We use $\mathcal{S}/\overline{\mathcal{S}}$ to denote the measure for (conventional) figure/background area respectively.

3 Convexity Measurement

To examine the orientation model and the Kullback-Liebler measure, we conduct different set of experiments. One set of images refers to the F/G separation task and we test ability of the model to account for human visual perception. The second set displays shape figures and the task is to order and compare them. For each set of examples we illustrate the results with several prototypes. The prototype illustrations for the F/G set are Fig. 4, Fig. 5 and Kanizsa's figure of comparing convexity versus symmetry (Fig. 6). The prototypes for the second set are a (non-) perfect ellipse and a "bell" shape (shown on the right-hand side of Fig. 7).

In Sec. 4, we consider another set studying behavior of the model as we vary the parameter κ. This is particularly important to understand how the shape size plays a role in the model.

We are also interested in the convexity comparison of perfectly convex shapes. Shapes like circles, squares, and triangles are lined up by the Kullback-Liebler measure. Also, the comparison of squares to rectangles will favor squares than rectangles. They will be shown in Sec. 5.

In all cases we used synthesized binary images. The parameters we used are, the decay coefficient $\lambda = 0.1/|\Omega|$, divided by area of the region Ω and the deviation factor $\kappa = 0.4$ except in the cases that are said otherwise. The peak of the delta function is simulated by $1/\varepsilon$ with $\varepsilon = 10^{-5}\cdot|\partial\Omega|$, a constant normalized by the perimeter of Ω. The

(a) (b)

Fig. 4. A simple experiment used for F/G separation and its relative entropy $D(P_{\mathbf{x}}\|Q)$. While right side is convex and left side is concave, we have $\mathcal{S}/\overline{\mathcal{S}} = \mathbf{0.605}/0.671$ respectively. Both regions are equally sized.

normalization of the parameters λ or ε according to area or perimeter of Ω respectively is not essential for the convexity measurement and can be removed.

3.1 Convexity as Salience

We test our measure for various prototypes. For a simple test in Fig. 4, the measure is given by $\mathcal{S}/\overline{\mathcal{S}} = \mathbf{0.605}/0.671$, favoring the white region. For another F/G image in Fig. 5, we have the consistent predictions through images with different ratios of bk/wt area. Also, we do observe the size effect from (a) to (c): the differences between figures and background become less as black/white regions get smaller/larger respectively. For a Kanizsa figure in Fig. 6(a3) where the white regions own the biggest area among (a1)-(a3), the result predicts that the white regions (convexity) prevail as the figure over the black regions (symmetry) with $\mathcal{S}/\overline{\mathcal{S}} = \mathbf{0.490}/0.497$. It can not be given by the model provided by [16] which gives $\mathcal{S}/\overline{\mathcal{S}} = 0.715/\mathbf{0.645}$, saying that the black regions will be figures and it is a “wrong” prediction.

The reason is that the decay model provided by Pao et al. [16] is too sensitive to the size and can not provide consistent predictions when we move the edge boundaries leftward or rightward, even the change is small and beyond the detection from our eyes. A better model, the oriented one will give correct predictions consistently, with shift of the edge boundaries.

4 Convexity versus Size

In the Euler-Lagrange equation in Eq. 9, the deviation factor κ serves as the diffusivity in the orientation space Θ. In the random walk formulation, a larger κ provides more noise and less deterministic behavior in orientation when it moves from one location to another neighboring location. A measure with small size preference is yielded in such a situation. On the other hand, a smaller κ has more control in orientation. The measure will have less size preference and be closer to ideal convexity measure than the one given in the less-deterministic case. The most extreme case gives the size invariance measure, provided by letting $\kappa \to 0$. It will be discussed later. Results related to different choices of κ will be studied in Sec. 4.1 for F/G separation and Sec. 4.2 for shape convexity comparison respectively. The choice of κ provides the flexibility of choosing convexity measure between a size-invariant one and the one with small size preference. It cannot be achieved by the decay measure in [16]. We use the Kanizsa images in Fig. 6 (Sec. 4.1) and the ellipse/bell pair in Fig. 7 (Sec. 4.2) to illustrate our idea.

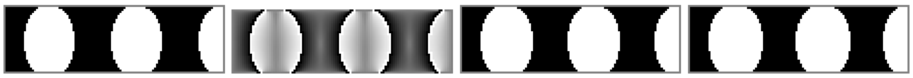

(a) $\mathbf{0.520}/0.587$ (a1) (b) $\mathbf{0.522}/0.585$ (c) $\mathbf{0.525}/0.583$

Fig. 5. Colonnade with boundaries translated through the horizontal direction from (a), a size balanced one to (c), with white regions owning the largest area. The relative entropy of (a) is shown in (a1). Their differences between the measures in figure/ground get smaller from (a) to (c), as black/white regions get smaller/larger. It shows the size/proximity preference of the model.

Size Invariance by Letting $\kappa \to 0$ Let us analyze the case when $\kappa \to 0$, where the walk is totally deterministic in orientation. By taking the limit $\kappa \to 0$, the functional in Eq. 8 becomes

$$\lim_{\kappa \to 0} \mathcal{H}(\sigma|\mathbf{x};\theta) = \frac{4}{\pi}(\cos\theta\,\sigma_x + \sin\theta\,\sigma_y)^2 .$$

We want to examine the effect of shape scaling in this limit for the whole functional in Eq. 7. After that, we study the scaling effect on the convexity measure $\mathcal{S}$.

Given two *similar* shapes Ω and Ω' in an image $\mathbf{I}$, indicated by two characteristic functions χ and χ' s.t. $\chi(\mathbf{x}) = 1$ or $\chi'(\mathbf{x}) = 1$ if $\mathbf{x} \in \Omega$ or Ω' respectively, and $\chi(\mathbf{x}) = 0$ or $\chi'(\mathbf{x}) = 0$ otherwise. Under an appropriately chosen coordinate system, we have $\chi(\mathbf{x}) = \chi'(r\mathbf{x}) = \chi'(\mathbf{x}'), \ \forall \mathbf{x}, \mathbf{x}' \in \mathbf{I}$. Given similar edge maps $e(\mathbf{x};\theta) = e'(\mathbf{x}';\theta) = |\mathbf{u}_\theta \cdot \mathbf{n}(\mathbf{x})|$, when $\kappa \to 0$ and $\lambda \to 0$, the decay term will vanish and we have

$$E(\sigma') = E(\sigma) = \int_{\Omega\times\Theta} \delta_2 \cdot e \cdot (\sigma - \sigma_0)^2 + \frac{4}{\pi}(\cos\theta\sigma_x + \sin\theta\sigma_y)^2 \, d\mathbf{x}\, d\theta ,$$

if we assign $\sigma'(\mathbf{x}';\theta) = \sigma(\mathbf{x};\theta)$. So the minimizer for either functional can be obtained easily when the other one has been computed. Two minimizers are related by $\sigma^*(\mathbf{x};\theta) = \sigma'^*(\mathbf{x}';\theta)$. Different orientations are worked independently here.

Let us discuss the scaling effect on the convexity measure. For two similar maps σ^*, σ'^*, we can obtain the similarity between $P_\mathbf{x}$ and $P_{\mathbf{x}'}$ or $D(P_\mathbf{x}\|Q)$ and $D(P_{\mathbf{x}'}\|Q)$. Therefore, for the convexity measure, we have

$$\mathcal{S}(P_{\mathbf{x}'}) = -\frac{1}{|\Omega'|}\int_{\Omega'} D(P_{\mathbf{x}'}\|Q)\, d\mathbf{x}' = -\frac{1}{r^2|\Omega|}\cdot r^2 \int_{\Omega} D(P_\mathbf{x}\|Q)\, d\mathbf{x} = \mathcal{S}(P_\mathbf{x}) .$$

It is an ideal case where we can achieve a measure with no sensitivity to the size. Examples in the discrete case can be found in Fig. 7 and Sec. 4.2. When λ is not zero, we need to set a new $\lambda' = \lambda/r^2$ to achieve the similarity $\sigma^*(\mathbf{x};\theta) = \sigma'^*(\mathbf{x}';\theta)$.

4.1 Figure/Ground Separation in Convexity-Symmetry Image and Tuning of κ

We will use the Kanizsa figures in Fig. 6 to illustrate our points. As we have discussed, the decay model cannot provide a consistent prediction when the area ratio of different regions is changed, even though the change is small and beyond the detection from our eyes. The orientation model will give a consistent prediction, with a small shift of the edge boundaries. The trick lies in the free parameter κ which on one hand (small κ or the extreme case with $\kappa \to 0$) gives a convexity measure without considering small size preference and on the other hand (big κ) gives a measure with the size preference. In Tab. 1, we have series (a1), balanced area for black and white regions, series (a2), larger white regions and (a3) white regions with the largest area. Several pairs of comparisons can be studied. When $\kappa = 0.1$, the purest convexity measure among them, gives the expected answer with white in the front, for all three cases. When $\kappa = \pi/2$, a case blended with the most size preference among them, white regions in (a1) & (a2) are preferred, but not for (a3) where the smaller black regions are preferred. The case of $\kappa = 0.4$ gives an intermediate transition. For the perceptual simulation, suppose a case where F/G is decided by both of the convexity and size preferences, we can tune the parameter κ to obtain the appropriate normalization of them, according to the preferences in human visual systems.

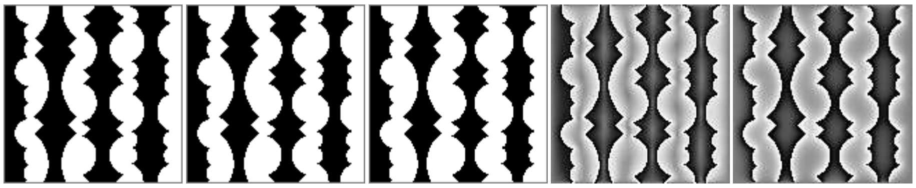

(a1) (a2) (a3) (b3) **0.490**/0.497 (c3) 0.653/**0.576**

Fig. 6. Convexity measure for the Kanizsa figures (adapted from Kanizsa [9]). (b3) gives the relative entropy of (a3) and (c3) gives the decay diffusion field of (a3) (Pao et al. [16]). When the boundaries are translated from (a1) to (a3) with white regions getting bigger, the convexity measure from the orientation diffusion gives $\mathcal{S}/\overline{\mathcal{S}} = \mathbf{0.490}/0.497$ in (b3), by a test of $\kappa = 0.1$ while in (c3), the measure from the PGR model shows $\mathcal{S}/\overline{\mathcal{S}} = 0.653/\mathbf{0.576}$, a "wrong" prediction. Note that the (non-oriented) decay diffusion process will have more diffusion near the neck area while in (b3), a bad relative entropy will be given with help of the oriented process. More discussion related to size and the choice of κ can be seen in Tab. 1.

Series (Area)	$\kappa = 0.1$	$\kappa = 0.4$	$\kappa = \pi/2$	Remark
Convexity Measure by Orientation Diffusion ($\mathcal{S}/\overline{\mathcal{S}}$)				
(a1) (+0/−0%)	**0.487**/0.502	**0.490**/0.499	**0.560**/0.570	size balanced
(a2) (+6/−0%)	**0.488**/0.500	**0.492**/0.497	**0.564**/0.565	
(a3) (+28/−0%)	**0.490**/0.497	0.495/**0.491**	0.573/**0.555**	
Convexity Measure by PGR model ($\mathcal{S}/\overline{\mathcal{S}}$)				
(a1) (+0/−0%)	**0.621**/0.653			size balanced
(a2) (+6/−0%)	0.638/**0.635**			
(a3) (+28/−0%)	0.671/**0.597**			

Table 1. Kanizsa figures with various size ratios (Fig. 6), measured by the orientation diffusion and the PGR model [16]. The series from (a1) to (a3) gives the white region area from small to large. Series (a1) has balanced size. For the orientation diffusion, a smaller κ gives a purer convexity measure and a larger κ, meaning more uncertainty in orientation in walks, will cause a stronger size preference. The prediction for F/G is likely to be decided by convexity when κ is small and be decided by size/proximity when κ is large. We can get convex predictions for F/G when $\kappa \leq 0.1$. The measure collected by the PGR model (result of (a3) is shown in Fig. 6(c3)) is pretty much a size measure if we do not provide a size-balanced experiment.

4.2 Convexity Comparison of Shapes and Tuning of κ

We study our convexity measure for different shapes with the same or different sizes. As shown in Fig. 7, the imperfect ellipses $A1$(large) & $A2$(small) represent convex shapes, and the bell shapes $B1$(large) & $B2$(small) represent non-convex shapes with "strong proximity" in the neck area. For the choice of κ, a similar scenario is used as in the F/G separation experiments. When κ is small, we pick shape by convexity and when κ is larger, we either pick the smaller size shapes or pick the bell shape with stronger proximity. The details are shown in Fig. 7.

Convexity comparison of shapes with the same size When two shapes share the same size, we can easily pick up the ellipse as the more convex shape by choosing $\kappa \leq 0.6$.

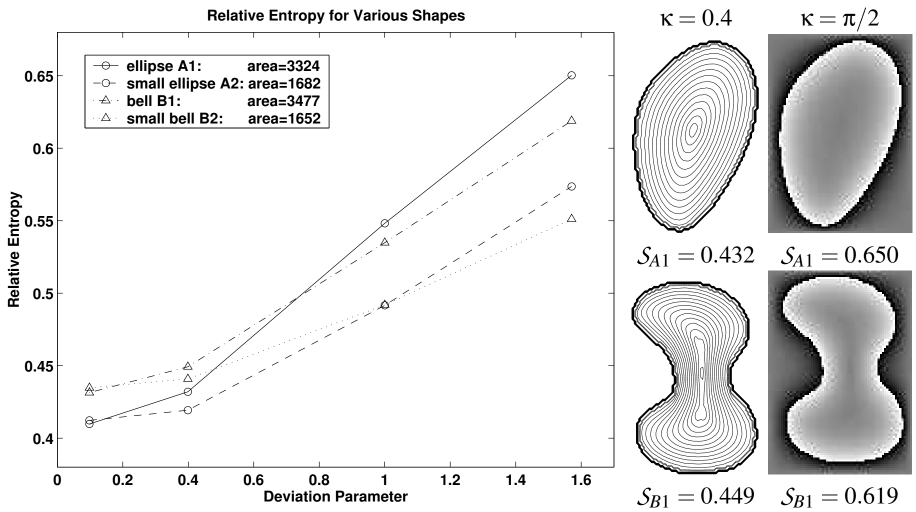

Fig. 7. A comparison between shapes with different sizes and convexity. Four curves listed in $\kappa = \pi/2$, from top to bottom are for the (imperfect) ellipse $A1$, bell $B1$, small ellipse $A2$ and small bell $B2$ (shapes A1, B1 are shown on the right). A measure with small κ will pick shapes by convexity. A measure with large κ will pick shapes by size/proximity; therefore, either small sized shapes or the bells which own strong proximity near the neck will be favored. When $\kappa = 0.1$, the case with the least size preference, the measures for all similar shapes with different sizes will coincide with each other. The level sets or the relative entropy for A1 and B1 with the simulations of $\kappa = 0.4$ and $\kappa = \pi/2$ are shown on the right-hand side. The preference between the ellipse and bell switches as we goes from a small κ to a large κ.

A large κ will favor proximity and therefore pick the bell as the more favorable shape. We have $\mathcal{S}_{A1} < \mathcal{S}_{B1}$ and $\mathcal{S}_{A2} < \mathcal{S}_{B2}$ when $\kappa \leq 0.6$.

Convexity comparison of shapes with any sizes To make the measure capable to be applied in a wider range, we compare shapes with different sizes, achieved by using an even smaller $\kappa \leq 0.4$. In this case, no size/proximity issues need to be considered and the measure becomes a "convexity measure". We have $\mathcal{S}_{A1}, \mathcal{S}_{A2} < \mathcal{S}_{B1}, \mathcal{S}_{B2}$ if $\kappa \leq 0.4$ is provided. The smallest κ or $\kappa = 0.1$ provides a measure with the least sensitivity to the size. As we can see, the values of similar shapes with different sizes are coincided to each other in this situation.

Large κ and size/proximity preference When κ is large, it is the case of diffusion with low certainty in orientation. We will have the result favoring smaller size shapes, as we have $\mathcal{S}_{\mathrm{A2}}, \mathcal{S}_{\mathrm{B2}} < \mathcal{S}_{\mathrm{A1}}, \mathcal{S}_{\mathrm{B1}}$. When similar size shapes are compared, a shape with stronger proximity will prevail. Therefore, the bell $B1$ is favored over the ellipse $A1$ and $B2$ is favored over $A2$, by having smaller measures.

5 Comparison of Convex Shapes

5.1 From Rectangle to Square

In Fig. 8, we run the model on a series of rectangles with ratio of side length from 0 to 1. As shown in the experiments, the closer to square the rectangle is, the better the convexity measure. The strong symmetry in the thin rectangles will be cancelled by the computation of Eq. 11.

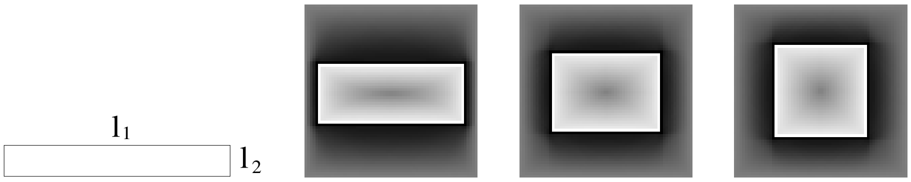

(a) (b) $\mathcal{S} = 0.437$ (c) $\mathcal{S} = 0.420$ (d) $\mathcal{S} = 0.417$

Fig. 8. (a) rectangle with ratio $l1$ to $l2$. (b) (c) (d) samples of different ratios $l2/l1$ and the relative entropy $D(P_{\mathbf{x}}||Q)$. Their measures are shown, given the parameter $\kappa = 0.1$.

5.2 From Triangle to Circle

In Fig. 9, we examine various regular shapes. Unlike the model provided by [16] giving a measure with the preference from triangle to circle, this orientation model gives a reverse order, prefers circle most, then, hexagon and triangle. By using the Kullback-Leibler measure, diffusion from neighboring inducers with *similar orientations* will accumulate around direction of the resulting vector θ^*, hence, giving a good score. For a cross check, the square in Fig. 8(d) has $\mathcal{S}_{\text{hexagon}} < \mathcal{S}_{\text{square}} < \mathcal{S}_{\text{triangle}}$, falling between the triangle and hexagon. A preference similar to the one given by the PGR model [16] can be achieved by a simulation with a large κ.

5.3 Convexity is different from Shape Compactness

It is interesting to compare our measure with the compactness CP generally given by $\text{CP}(\partial\Omega) = |\partial\Omega|^2/(4\pi \cdot |\Omega|)$. As we can easily find out, the same preference for regular shapes and the preference of squares over rectangles are also established by the compactness CP. However, the difference between them is shown in various viewpoints:

1. Unlike the shape convexity, the compactness will favor a region with large area instead of small area provided regions with the same perimeter. However, the small size preference does exsit in F/G selection, which can be simulated by our convexity measure (Fig. 5, Fig. 6 and Tab. 1).
2. A circle-like shape with fine scale perturbation may have larger compactness than a smooth-boundary, non-circular shape (Young et al. [21], Bribiesca [2], Fig. 10 (a) & (b)).

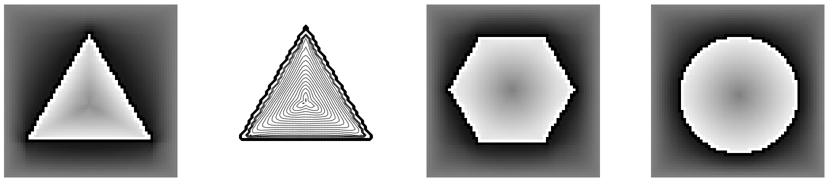

(a) $\mathcal{S} = 0.422$ (b) $\mathcal{S} = 0.410$ (c) $\mathcal{S} = 0.407$

Fig. 9. The relative entropy or corresponding iso-contours derived by our orientation process. Their measures are shown, with the parameter set to be $\kappa = 0.1$. Note that the square in Fig. 8(d) falls between triangle and hexagon. The area information is provided as (a) triangle: 897, (b) hexagon: 1361, and (c) circle: 1469 pixels.

3. Our measure has the flexibility to switch between a size-invariant convexity measure or one with small size preference. Also, the freedom to choose the preference of circles over triangles (small κ) or triangles over circles (large κ), etc.
4. It is hard to generalize the shape compactness in the applications where the shape is partial or occluded.

Some examples to illustrate the difference between the compactness and the convexity can be shown in Fig. 10. For the shape (a), perturbations in the fine scale cause a smaller change in the convexity measure, than in the compactness.

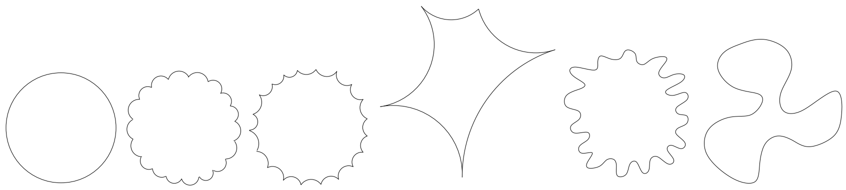

$\mathcal{S} =$	0.404	0.406	0.411	0.425	(a) 0.437	(b) 0.440
CP =	1.000	1.321	1.528	2.788	3.152	2.917

Fig. 10. Convexity measure for various shapes with different convexity in different scales, from the most convex to the least convex one ($\kappa = 0.1$).

6 Symmetry Information

The idea that symmetry can be captured by our model is not particularly new or surprising. For example, based on the work of Siddiqi and Kimia [19], we know that the diffusion process over shapes will "meet" (yield shocks) at the symmetry axis. What is particular to our work, is that the diffusion is on the space $\mathbf{R}^2 \times \mathbf{S}^1$ and presented by a vector form, so the symmetry information can be extracted by a local computation method.

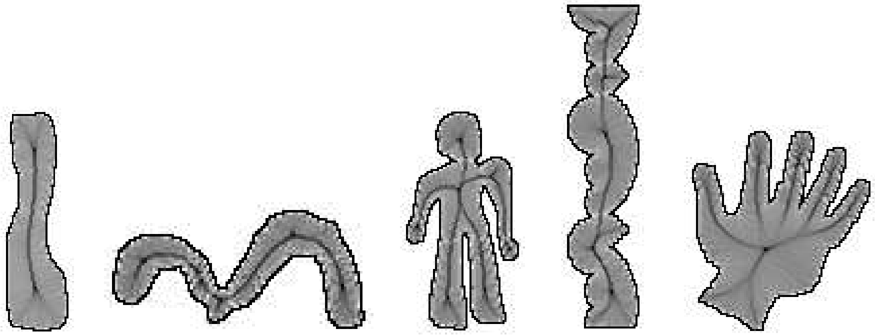

Fig. 11. Shape axis σ^*_{sym} (Eq. 14), computed by using the maximum vector σ^*_M, with $\kappa = \pi/2$.

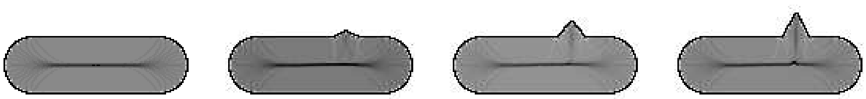

Fig. 12. Shape axis with a protrusion on boundaries. We have the transition from (b1) ignored, (b2) having "sub-axis" to (b3) disturbing the main axis by a faction. We choose the maximum vector $\hat{\sigma}^*_M$, and select the deviation factor $\kappa = \pi/2$.

Let us collect the maximum vectors $\sigma^*_M(\mathbf{x})$ by

$$\hat{\sigma}^*_M(\mathbf{x}) = \sigma^*(\mathbf{x};\theta_M)\cdot\mathbf{u}_M \qquad \text{where} \qquad \sigma^*(\mathbf{x};\theta_M) = \max_{\theta\in[0,2\pi)}\{\sigma^*(\mathbf{x};\theta)\},$$

with $\mathbf{u}_M = (\cos\theta_M, \sin\theta_M)$. We would like to examine the field

$$\sigma^*_{\text{sym}} = \operatorname{div}\left(\frac{\hat{\sigma}^*_M}{\|\hat{\sigma}^*_M\|}\right). \tag{14}$$

The *shape axis* (different from the conventional symmetry axis [15]) is viewed as the place with most sinkage, in the normalized map of the maximum vectors. The map shows "how likely" a point can be on any axis or "how strong" the axis is. Examples of shape axis can be found in Fig. 11.

6.1 Protrusion

To see what protrusion or noise on boundaries can affect the shape axis, we study the axes of shapes in Fig. 12. In (b1), the main axis stays the same as we perturbing the boundaries from (a) by a small protrusion. But a larger effect can (b2) eventually produce a new axis or (b3) even change location of the main axis. By this representation, any further pruning of the "sub-axis" will not be necessary. Because sub-axes are given in "lighter" representations and can be easily removed.

7 Conclusion

We have proposed a framework to capture critical shape information: namely convexity, symmetry and size. It is an orientation diffusion approach, rooted in Markov random fields. The focus of the paper was on demonstrating how the model evaluates convexity, and how size is integrated into the model depending upon a parameter κ. Although it is not surprising, we have indicated how symmetry can also be captured. The protrusion effect on boundaries was naturally solved by this approach. We have demonstrated the validity of the model on various examples and how it improves on previous works. We believe that this approach provides a wealth of information on shapes, and thus, will be used by other practitioners.

References

1. D. H. Ballard and C. M. Brown. *Computer Vision*, Prentice-Hall, New Jersey, 1982
2. E. Bribiesca. "Measuring 2D Shape Compactness using the Contact Perimeter", *Computers and Mathematics with Applications*, **33**(11): pp. 1–9, 1997.
3. V. Bruce, P. R. Green and M. A. Georgeson. *Visual Perception, Physiology, Psychology, and Ecology* (3rd ed.), Psychology Press, 1996.
4. P. Dimitrov, C. Philips and K. Sidiqi. "Robust and efficient Skeletal graphs", *CVPR*, South Carolina, June, 2000
5. D. Geiger, H. Pao and N. Rubin. Salient and multiple illusory surfaces. *Computer Vision and Pattern recognition*, June. 1998.
6. F. Heitger and R. von der Heydt. A computational model of neural contour processing: Figure-ground segregation and illusory contours. *Proceedings of the IEEE*, pp. 32–40, 1993.
7. D. Huttenlocher and P. Wayner, "Finding Convex Edge Groupings in an Image," *International Journal of Computer Vision*, **8**(1): pp. 7–29, 1992.
8. D. Jacobs. Robust and efficient detection of convex groups", *IEEE Trans. PAMI*, 1995.
9. G. Kanizsa. *Organization in Vision*. Praeger, New York, 1979.
10. B. Kimia, A. Tannenbaum, S. Zucker. "Shapes, Shocks, and Deformations I: The components of two-dimensional shape and the reaction-diffusion space", *Int. J. Comp. Vis.* **1**: pp. 189–224, 1995.
11. K. Koffka. *Principles of Gestalt Psychology*. New York: Harcourst. 1935.
12. K. Kumaran, D. Geiger, and L. Gurvits. Illusory surfaces and visual organization. *Network: Comput. in Neural Syst.*, **7**(1), Feb. 1996.
13. D. Mumford. Elastica and computer vision. In C. L. Bajaj, editor, *Algebraic Geometry and Its Applications*. Springer-Verlag, New York, 1993.
14. M. Nitzberg and D. Mumford. The 2.1-d sketch. In *ICCV*, pp. 138–144, 1990.
15. H. Pao. "A continuous model for shape selection and represenation", PhD thesis, 2001.
16. H. Pao, D. Geiger and N. Rubin. "Measuring convexity for figure/ground separation", *Int. Conf. on Comp. Vis.*, pp. 948–955, Sep. 1999.
17. S. Parent and S. W. Zucker, "Trace inference, curvature consistency and curve detection", *IEEE PAMI*, Vol. 11, No. 8, pp. 823–839, 1989.
18. E. Rubin, *Visuell wahrgenommene Figuren*, (Copenhagen: Gyldendals), 1921.
19. K. Siddiqi and B. B. Kimia. "A shock frammar for recognition", *Computer Vision and Pattern recognition*, 1996.
20. B. Tang, G. Sapiro and V. Caselles. "Direction diffusion", *International Conference on Computer Vision*, Sep. 1999.
21. I. Young, J. Walker and J. Bowie. "An Analysis technique for biological shape", *Information and Control*, **25**: pp. 357–370, 1974.